ISBN: 978-3-95450-256-1 ISSN: 2673-5504 doi: 10.18429/JACoW-SRF2025-WEA06

PERFORMANCE OF THE CORNELL CONDUCTION-COOLED Nb_3Sn CRYOMODULE (C4M)*

J. Parsons†, N. Stilin‡, H. Conklin, T. Gruber-Hine, A. Holic, G. Kulina, M. Liepe, P. Quigley, J. Sears, V. D. Shemelin, J. Turco, CLASSE, Cornell University, Ithaca, NY, USA

Abstract

Recent improvements in Nb_3Sn cavity and commercial cryocooler performance have made conduction-cooled cryomodules for SRF cavities feasible, which drastically expands SRF applications, e.g., to medical imaging, water purification, and security. Cornell has developed a turnkey, conduction-cooled cryomodule to operate a 1.3 GHz Nb_3Sn SRF cavity by optimizing the cooling output of two commercial cryocoolers. The cryomodule, cavity, and RF input coupler have been designed for very high continuous wave (CW) beam current operation (>100 mA) and high RF power (100 kW per coupler). We present the design, optimization, and assembly process of this conduction-cooled cryomodule as well as performance during initial cool down tests and low power RF testing.

INTRODUCTION

Cryocooler technology provides an alternate cooling scheme for SRF cavities to modern cryoplants that takes advantage of Nb_3Sn's relatively high operating temperature of 4 K [1–9]. Without using liquid cryogens, operating these machines requires minimal cryogenic knowledge and expertise, which vastly expands the pool of potential operators outside of academic settings. With lower operating costs, easier and infrequent maintenance, and turnkey capability compared to cryoplants, cryocooled SRF technology offers solutions to small-scale operations that may not warrant the commissioning of full-scale cryoplants. This new branch of SRF technology can then be applied to water purification, soil decontamination, medical isotope production, security imaging, biofuel production, and many more non-academic fields [10, 11]. However, it is important to note that the beam demands of small-scale SRF operation are typically high for one cavity to produce: MEC-scale beam energy, >100 mA of beam current, and MW-scale of average beam power.

Despite the draw of cryocooled SRF cryomodules, technological developments in the past decade have only recently allowed for progress in these cryomodules. 1.3 GHz Nb_3Sn cavities now reliably dissipate <1 W of heat per cell when operated at accelerating gradients of 10 MV/m with quality factors on the order of 10^{10}. Likewise, cryocoolers now reliably extract >5 W of heat at 4 K [12], which provides a tight but usable cooling power budget with which to design a conduction-cooled cryomodule for small-scale operation. Moreover, a proof-of-principle demonstration of a cryocooled 2.6 GHz Nb_3Sn cavity at Cornell concluded that a cryocooled cavity can achieve accelerating gradients of 10 MV/m [13]. This experiment also showed that cryocooled cavities require well controlled controlled cool downs when cooled through T_c to minimize thermoelectric currents, which may eventually be automated with heater PID loops for full turnkey capabilities.

This project focused on the design, assembly, and testing of Cornell's first conduction-cooled cryomodule (C4M for short). C4M uses two pulse tube cryocoolers – 1 Cryomech PT420 and 1 Cryomech PT425 – which output a combined cooling power of 4.15 W at 4 K and 100 W at 45 K. The design phase emphasized ways to reduce static and dynamic heat loads across a newly fabricated conduction-cooled cavity during >100 kW operation. The assembly phase details the process and challenges associated with the first ever assembly of C4M starting in the clean room. Finally, the testing phase concerns the thermal and RF performances of C4M's first cool down along with development of a controlled cool down procedure for maximizing the cavity's RF performance.

CRYOMODULE DESIGN

Conduction-Cooled Cavity

Contemporary SRF cavity designs do not readily facilitate conductive thermal links, so the Cornell cryomodule team carefully considered their approach to fabricate a new conduction-cooled cavity. This 1.3 GHz Nb_3Sn cavity's equator and beam tube transitions were modeled after the two-cell ILC cavity for Cornell's Energy Recovery Linac [14]. Four Nb rings – two welded to the cavity and one welded to each beam tube transition – allow for surface-surface coupling between the cavity and thermal transporting pieces [15] as seen in Fig. 1. Two forward power coupling ports were installed along the small beam tube for future coupler operation. The cavity was designed to perform with $Q = 10^{10}$ with $E_{acc} = 10$ MV/m at 4 K.

The cavity's heat intercepts and thermal links are optimized to minimize thermal gradients both across the cavity and between the cavity and cold heads during high power operation. All simulations were performed with 1.5 W of heat dissipated at the high magnetic field region on the cavity's equator: 1 W of heat for typical dissipation on a 1.3 GHz cavity and 0.5 W as a safety factor. Notably, the temperature gradient across the cavity was kept below 50 mK [15]. Detailed results from these simulations are compared to measured values in Table 1 within the "Thermal Links" subsection.

* This work was supported by U.S. DOE award DE-SC0021038 "Next Steps in the Development of Turn-Key SRF Technology."
† jrp356@cornell.edu
‡ Currently at Jefferson Lab, Newport News, USA

ISBN: 978-3-95450-256-1 ISSN: 2673-5504 doi: 10.18429/JACoW-SRF2025-WEA06

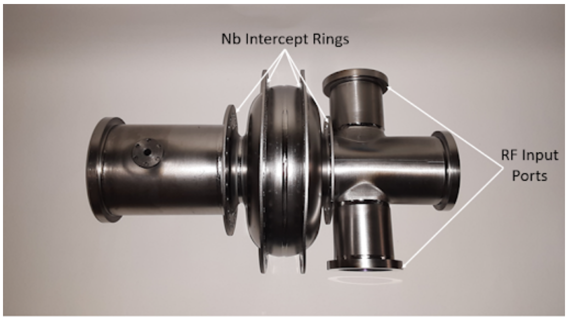

Figure 1: Cornell's first newly-fabricated conduction-cooled cavity, with Nb rings and forward coupler ports highlighted.

RF Coupler

A conduction-cooled RF coupler capable of transferring 100 kW CW RF power into the cavity was developed to contend with high power demands for small scale SRF applications [16]. Its base design drew inspiration from Cornell's ERL injector [14], and the RF shield design was based on work from Fermilab [17]. Each coupler is designed to dissipate 1.11 W at 4 K and 37.90 W at 45 K when applying 100 kW of power into the cryomodule. One such coupler is currently being manufactured with assembly on the cryomodule slated for late 2026.

Cryostat

Along with the highly optimized cavity and couplers, every remaining mechanical connection to the cavity and cold heads was scrutinized to minimize additional heat loads [18]. To address remaining static and radiative heat loads in particular, an Al space frame was placed around the cavity to aid with beam line suspension and installing a thermal shield. Four G10 rods attached to each beam tube suspend the cavity from the space frame, and an additional eight rods suspend the space frame within the vacuum vessel. G10 was chosen for its high tensile strength but low thermal conductivity compared to stainless steel, decreasing the static heat load to approximately 0.25 W.

Moreover, an Al thermal shield was installed around the space frame, which conductively couples to the beam tubes as well as the cold head first stages via copper thermal straps. With both couplers operating at 100 kW, the thermal shield is expected to maintain a temperature of 45 K to cool the beam tubes and couplers in future experiments. The radiative heat load on the cavity is predicted to decrease from ~10 W to ~0.1 W while the thermal shield is cold.

ASSEMBLY PROCESS

C4M's assembly process can be partitioned into three main parts: the clean room assembly (where the cavity and beam line are placed inside the cryomodule vacuum vessel), the 4 K assembly (which deals with connections made on the cavity), and the 45 K assembly (which largely involves the outer-lying Al thermal shield).

Clean Room Assembly

After the cavity received its workup and tin coating [18], stainless steel beam tube extensions were attached to the cavity. A low power, high external Q input antenna was installed at one of the RF input ports, and a pickup probe was placed on the large beam tube. Then, the cavity was suspended from the space frame via the G10 rods before the space frame was placed inside of the vacuum vessel. The thermal and magnetic shield panels that intersect the beam line were installed at this stage. The beam tube extensions are then coupled to the vacuum vessel via bellows to complete the beam line. An overhead view of the complete clean room assembly is shown in Fig. 2.

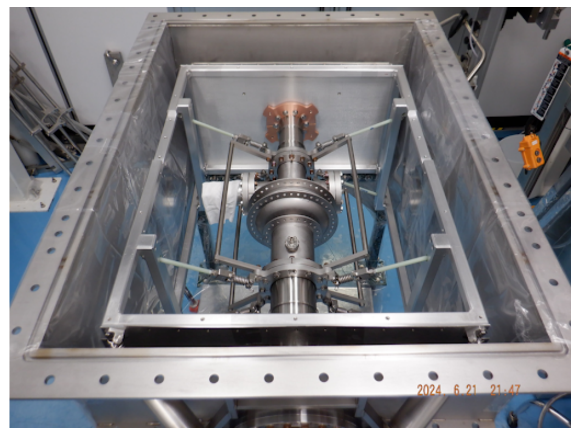

Figure 2: Full cavity and beam line suspension in vacuum vessel using Al space frame and G10 rods.

4 K Assembly

The first portion of post-clean room assembly deals with conductively coupling the cold heads' second stages to the cavity via the Nb rings. Each Nb ring has two 5N Al split rings fastened transversely along their lengths to form one complete thermal link per Nb ring. Two high-conductivity copper thermal straps are fastened to each equator split ring, and one strap is attached to each beam tube split ring. Then, on either transverse side of the cavity, each set of six thermal straps is bolted to a 5N Al plate, upon which the cold head second stages will be secured to deliver cooling power to the cavity as shown in Fig. 3. An additional high conductivity copper thermal strap with a copper antenna clamp was run from the 5N plate to the antenna feedthrough. All 4 K conductive connections use indium foil as a surface-surface intermediate, except the antenna clamp connection which uses thermal grease.

RTD Cernox sensors are placed along the cavity, beam tubes, and 5N Al plates for added resolution of system temperatures and gradients. Attached to each split ring set is a heater consisting of two resistors that allow for longitudinal temperature control. Where necessary, all instrumentation surface contacts use thermal grease to establish thermal contact, but the 4 K copper RF cable thermal anchors use indium foil between itself and the 5N plate.

ISBN: 978-3-95450-256-1 ISSN: 2673-5504 doi: 10.18429/JACoW-SRF2025-WEA06

Figure 3: Post-clean room assembly of 5N Al split rings and 5N Al plates to be coupled to cold head second stages.

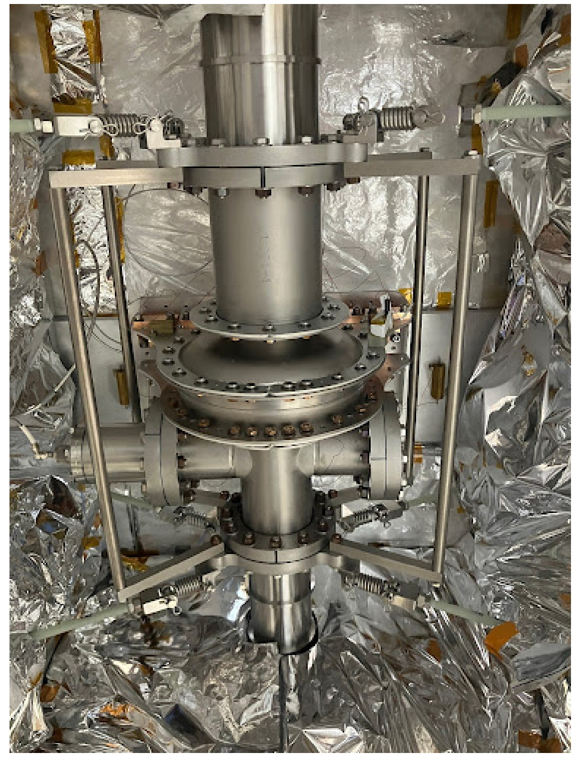

Figure 4: Internal view from below of cavity and full thermal and magnetic shielding.

45 K Assembly

This section of the assembly deals with coupling the cold heads' first stages to the higher temperature intercepts along the beam tubes and the Al thermal shield. Four copper thermal straps were bolted from the beam tubes to the thermal shield. Once all of the second stage instrumentation was finalized, the remaining side and upper thermal shield panels were secured to the space frame, followed by magnetic shield panels on the aforementioned surfaces. Multilayer insulation was then fixed to the inner and outer surfaces of the space frame, with a picture of the complete internal view displayed in Fig. 4.

Four thermal straps per cold head were secured to the upper thermal shield to later be attached to copper heat sink mounts on the cold head first stages. Then, after placing the top vacuum plate for added support, the cold heads are lowered into the cryomodule, where the first stages are coupled to the upper thermal shield and the second stages are bolted to the 5N plates with an indium foil intermediate. Cernox sensors were placed along the upper thermal shield panel for first stage temperature readings, and the RF cables were thermally anchored to a heat sink mount. One heater was secured to the upper thermal shield. Finally, the bottom panels for the space frame shielding were attached along with MLI, and the rest of the vacuum vessel was closed to complete the assembly. On the 45 K assembly, all thermal and instrumentation connections use thermal grease as an intermediate.

COOL DOWN TESTING

First Cool Down

The primary goal of the first cool down was to characterize the baseline cold temperatures along the cavity, beam tubes, and first stage as well as the time required to cool to baseline cold. Thus, the first cool down began by turning on both cryocoolers and not interfering until the system reaches its baseline cold temperatures. The first 10 hours of cooling are shown in Fig. 5. The top two curves represent the beam tubes, which cooled down the slowest since they have the shortest thermal path to room temperature through the bellows. Their final temperature lied just above the largest group of sensors in the figure representing second stage pieces across the cavity and the 5N plates. Finally, the lone curve that cooled down the quickest at first was on the first stage. The cavity reached 4 K at the 19.3 hr mark, and the system reached its baseline cold temperature after roughly 24 hr. Also of importance: the temperature gradient across the cavity when crossing through $T_c = 18K$ was 890 mK, which is greater than the maximum gradient used in most Cornell Nb_3Sn RF tests. Therefore, a controlled cool down was required to optimize cavity performance.

Controlled Cool Down

To decrease the temperature gradient across the cavity as it was cooled through T_c, we attempted a slow controlled cool down using heaters present along the cavity to control the gradient. The heaters placed along each split ring allow

ISBN: 978-3-95450-256-1 ISSN: 2673-5504 doi: 10.18429/JACoW-SRF2025-WEA06

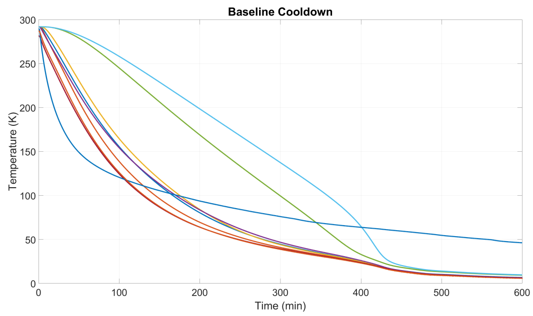

Figure 5: First 10 hours of C4M's first cool down. Three major groups of sensors are the beam tubes (top initial group), second stage/cavity (middle group), and first stage (bottom initial curve).

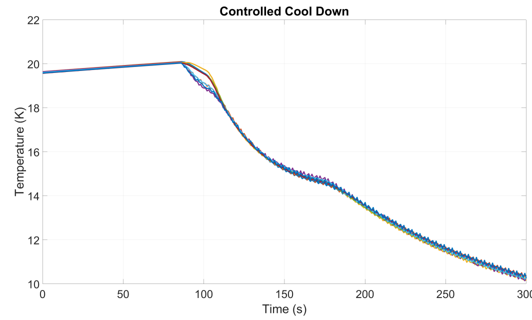

Figure 6: Fast controlled cool down characterization for current C4M setup. Cavity temperature gradient stays within 140 mK when cooled from 18.5 K to 16.5 K.

for longitudinal gradient tuning. Using these heaters, the longitudinal gradient was decreased below 100 mK. However, the transverse gradient could not be reduced to less than 300 mK. This was likely due to the different efficiencies of the cryocoolers, each of which were conductively coupled to either side of the cavity transversely. Due to the cold thermal shield surrounding the cavity as well as the isolation vacuum, cycling the more efficient cryocooler on and off changed the temperatures of each split ring by roughly 5 K in 30 s, so creating a slow controlled cool down procedure proved challenging given the short time frame before the conference.

We instead attempted a fast controlled cool down through T_c by taking advantage of this added sensitivity from cycling cryocooler power. Using Fig. 6 for reference: starting with both cryocoolers turned off, temperatures across the cavity increased with minimal gradient. Once the cavity reached 20.5 K, the weaker cryocooler was turned on to give its half of the cavity a head start, and the equator heaters were activated to prevent the equator from cooling down much quicker than the beam tubes. Then, after waiting 15 s, the stronger cryocooler was turned on, focusing the cavity temperatures as the cavity cooled from 18.5 K to 16.5 K in 15 s. Finally, after a satisfactory cool down through T_c, the equator heaters were turned off to allow the system to reach baseline cold temperatures again. Using this method, the temperature gradient across the cavity was reduced to 140 mK, which was acceptable for this first cryomodule test.

Thermal Links

The first row of Table 1 details the baseline temperatures longitudinally across the cavity as well as the beam tubes and cold head second stage. The baseline cavity and cold head temperatures were lower than the target temperature of 4 K, which is an important milestone in the development of the conduction-cooled cryomodule. The beam tube temperatures – especially on the large beam tube – were higher than the simulated values of ~4.6 K, but these recorded temperatures were still close to cavity temperatures near 4 K. Using the cryocooler efficiency curves for both cryocoolers as well as the temperatures of both cold head stages, the total static heat loads on the second and first stages were calculated to be < 2 W and < 40 W respectively, which are sufficiently small static loads for this system and another massive milestone reached in C4M's development.

To compare cavity temperatures and gradients during operation with the earlier simulated values, we applied 1 W of heat load across the cavity equator using the equator split ring heaters and compared the same set of temperatures to simulations with a 1.5 W heat load. Rows 2 and 3 of Table 1 correspond to the measured 1 W temperatures and simulated 1.5 W temperatures respectively. The measured temperatures and gradients align with the simulated values, which is another success for the first cool down. Though the temperature measured on the large beam tube ring was slightly higher than expected, we hope to address this discrepancy by modifying the beam tube extensions to lower the static heat load.

RF PERFORMANCE

Q vs E data was taken before and after the controlled cool down to compare to both each other and the baseline vertical test. Results from all three tests are presented in Fig. 7. As expected, Q increased after the controlled cool down was performed by roughly a factor of 3 since there was less trapped flux present in the cavity. The cavity performed on-par with the baseline vertical test after the controlled cool down. Thus, the cavity RF performance did not degrade from the vertical test to installation in the cryomodule, which is a success for the cryomodule's first assembly and cool down.

Multipacting bands were discovered during the cavity's baseline vertical tests, appearing at 3 MV/m and 7 MV/m after the tin coating was applied [18]. In C4M, multipacting began at roughly 3.5 MV/m during both RF tests, which prevented the acquisition of Q values at higher fields. Due to limited time to take data before the conference, we did not process through the first multipacting band to acquire Q vs E data above 3.5 MV/m. Processing will commence after the conference at low power to protect the sensitive RF cables for this setup. Likewise, fabrication of a new conduction-cooling cavity will begin later this year to pre-

ISBN: 978-3-95450-256-1 ISSN: 2673-5504 doi: 10.18429/JACoW-SRF2025-WEA06

Table 1: Second stage temperatures with various heat loads on beam tube (BT) and equator split rings, beam tubes, and cold heads. All reported values are averages from both sides of each section, the true values which differed by no more than 100 mK for each presented value.

Measurement Type	Large BT Ring	Equator 1	Equator 2	Small BT Ring	Beam Tube	Cold Head
Baseline	3.85 K	3.52 K	3.54 K	3.67 K	~5.05 K	3.46 K
1 W Dissipated	**4.45 K**	**4.35 K**	**4.38 K**	**4.33 K**	~6.41 K	4.05 K
1.5 W Simulated	**4.36 K**	**4.37 K**	**4.37 K**	**4.36 K**	~4.60 K	4.20 K

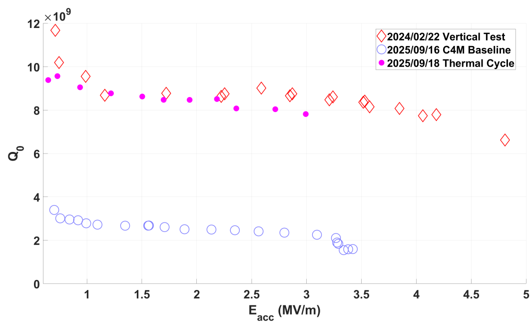

Figure 7: Q vs E plot comparing the cavity vertical test to cryomodule RF tests before and after thermal cycle.

vent multipacting issues in future cryomodule assemblies. Previous studies have shown that increasing the radius of curvature at the large beam tube transition may eliminate multipacting for this cavity geometry [19].

CONCLUSION AND FUTURE WORK

Ultimately, the first assembly and cool down of C4M met or exceeded expectations for thermal and RF performance. We carefully documented the cryomodule assembly process to facilitate quicker assemblies in the future. We extensively measured temperatures across the system to identify places of high heat loads to be addressed later, and we demonstrated that C4M's cavity performance aligned with the cavity's vertical test results. In the near future, the beam tube extensions will be scrutinized for modifications that can potentially decrease their static heat load; a new conduction-cooled cavity will be fabricated to eliminate multipacting; and preparations are under way to install the RF coupler for operation in early 2027.

ACKNOWLEDGMENTS

I would like to thank Dr. Neil Stilin and Prof. Matthias Liepe for their guidance, cryomodule and cavity design, and knowledge transferred when I picked up this project a little over a year ago. Thanks to the Cornell Cryomodule Team and the Cornell SRF technicians for their support and expertise in designing and assembling the cryomodule. Lastly, thanks to the CLASSE Cryo and Electrician Groups as well as Professors Mike Niemack, Abby Crites, Brad Ramshaw, and Jeevak Parpia for additional support with cryocooler operation.

REFERENCES

[1] S. Posen and M. Liepe, "Advances in development of Nb_3Sn superconducting radio-frequency cavities", *Phys. Rev. ST Accel. Beams*, vol. 17, p. 112001, Nov. 2014. doi:10.1103/PhysRevSTAB.17.112001

[2] S. Posen, "Understanding and Overcoming Limitation Mechanisms in Nb_3Sn Superconducting RF Cavities", Ph.D. dissertation, Phys. Dept., Cornell University, Ithaca, NY, USA, 2014. https://www.classe.cornell.edu/rsrc/Home/Research/SRF/SrfDissertations/Posen_thesis.pdf

[3] D. L. Hall, "New Insights into the Limitations on the Efficiency and Achievable Gradients in Nb_3Sn SRF Cavities", Ph.D. dissertation, Phys. Dept., Cornell University, Ithaca, NY, USA, 2017. https://www.classe.cornell.edu/rsrc/Home/Research/SRF/SrfDissertations/Daniel_Hall_PhD_Thesis_Final.pdf

[4] S. Posen, M. Liepe, and D. L. Hall, "Proof-of-principle demonstration of Nb_3Sn superconducting radiofrequency cavities for high Q0 applications", *App. Phys. Lett.*, vol. 106, p. 082601, 2015. doi:10.1063/1.4913247

[5] S. Posen and D. L. Hall, Nb_3Sn Superconcdcution Radiofrequency Cavities: Fabrication, Results, Properties, and Prospects", *Supercond. Sci. Technol.*, vol. 30, p. 33004, 2017. doi:10.1088/1361-6668/30/3/033004

[6] S. Posen *et al.*, "Advances in Nb_3Sn superconducting radiofrequency cavities towards first practical accelerator applications", *Supercond. Sci. Technol.*, vol. 34, p. 025007, 2021. doi:10.1088/1361-6668/abc7f7

[7] U. Pudasaini *et al.*, "Recent Results From Nb_3Sn Single Cell Cavities Coated at Jefferson Lab", in *Proc. SRF'19*, Dresden, Germany, Jul. 2019, pp. 65-70. doi:10.18429/JACoW-SRF2019-MOP018

[8] R. C. Dhuley, S. Posen, M. I. Geelhoed, O. Prokofiev, and J. C. T. Thangaraj, "First demonstration of a cryocooler conduction cooled superconducting radiofrequency cavity operating at practical cw accelerating gradients", *Supercond. Sci. Technol.*, vol. 33, p. 06LT01, 2020. doi:10.1088/1361-6668/ab82f0

[9] G. Ciovati *et al.*, "Development of a Prototype Superconducting Radio-Frequency Cavity for Conduction-Cooled Accelerators", presented at the SRF'23, Grand Rapids, MI, USA, Jun. 2023, paper THIXA04, unpublished.

[10] U.S. DOE Report, "Accelerators for America's Future", June 2010.

ISBN: 978-3-95450-256-1 ISSN: 2673-5504 doi: 10.18429/JACoW-SRF2025-WEA06

https://www.odu.edu/content/dam/odu/col-dept/physics/docs/report-future-cas.pdf

[11] U.S. DOE Report, "Workshop on Energy and Environmental Applications of Accelerators", Argonne, IL, USA, June 2015. https://www.osti.gov/servlets/purl/1358082

[12] Cryomech, https://www.cryomech.com/products/

[13] N.A. Stilin *et al.*, "RF and thermal studies on conduction cooled Nb_3Sn SRF cavity", *Eng. Res. Express*, vol. 5, p. 025078, 2023. doi:10.1088/2631-8695/acdd51

[14] V. Veshcherevich *et al.*, "Input Coupler for ERL Injector Cavities", in *Proc. PAC'03*, Venice, Italy, May. 2003, paper TPAB009, pp. 1201–1203. doi:10.1109/PAC.2003.1289652

[15] N.A. Stilin *et al.*, "Design and Commissioning of a New SRF Cavity for a Conduction-Cooled System", in *Proc. IPAC'23*, Venice, Italy, Jun. 2023, pp. 2987-2990. doi:10.18429/JACoW-IPAC2023-WEPA143

[16] N.A. Stilin *et al.*, "Design of a 1.3 GHz High-Power RF Coupler for Conduction-Cooled Systems", in *Proc. SRF'23*, Grand Rapids, MI, USA, Jun. 2023, pp. 342–346. doi:10.18429/JACoW-SRF2023-MOPMB094

[17] R. C. Dhuley *et al.*, "Design of a 10 MeV, 1000 kW average power electron-beam accelerator for wastewater treatment applications", *Phys. Rev. Accel. Beams*, vol. 25, p. 041601, 2022. doi:10.1103/physrevaccelbeams.25.041601

[18] N. A. Stilin, "Design and Commissioning of a Compact Conduction-Cooled SRF Cryomodule," Ph.D. dissertation, Cornell University, Ithaca, NY, USA, 2024. https://prod.classe.cornell.edu/sites/default/files/2025-07/Stilin_dissertation_d2-2.pdf

[19] S. Belomestnykh and V. Shemelin, "Multipacting-free Transitions Between Cavities and Beam-Pipes", *Nucl. Instrum. Methods Phys. Res. A*, vol. 595, pp. 293–298, 2008. doi:10.1016/j.nima.2008.05.041